

A Smooth Contact-State Transition in a Dynamic Model of Rolling-Element Bearings

Matej Razpotnik^a, Gregor Čepon^{a,*}, Miha Boltežar^a

^aUniversity of Ljubljana, Faculty of Mechanical Engineering

Abstract

We present a new formulation to calculate the response of a system containing rolling-element bearings operating under a radial clearance and a dominant radial load. The nonlinear bearing force- and stiffness-displacement characteristics in combination with the bearing clearance necessitate an advanced numerical analysis. The response of a shaft-bearing-housing assembly can be unstable in the transient regions, e.g., at the start of a system run-up or when passing the critical speed of a system. This can lead to long computational times or even to non-converged solutions. In this paper, a new analytical bearing-stiffness model is presented that is capable of overcoming these problems by smoothing the nonlinear bearing force- and stiffness-displacement characteristics in the discontinuous regions. The smoothing is implemented on the deformation scale. The proposed model is modular, allowing us to define a specific value of the smoothing to each rolling element that comes into contact. A simple case study that involves two bearings of different types (ball and cylindrical roller) is presented. They support an unbalanced rotor, subjected to a constant angular acceleration. We show that a small smoothing value can significantly enhance the numerical calculation of the chosen system in terms of speed and stability.

Keywords: Dynamic bearing model, Smooth contact-state transition, Rolling-element bearing stiffness matrix, Unbalanced rotor

Nomenclature

A_0	Unloaded distance between the inner and outer raceway grooves' curvature centres [mm]
A_j	Loaded distance between the inner and outer raceway grooves' curvature centres [mm]
D	Bearing outer diameter [mm]
d	Bearing inner diameter [mm]
F_i	Mean bearing force in the $i = x, y, z$ directions [N]
\mathbf{f}_b	Mean bearing load vector, composed by the mean bearing forces F_i and the mean bearing moments M_i ($i = x, y, z$).
K_n	Rolling-element load-deflection stiffness constant [N/mm ⁿ]
\mathbf{K}_b	Comprehensive bearing-stiffness matrix of dimension six
k_{ij}	Bearing stiffness coefficient, $i, j = x, y, z, \beta_x, \beta_y, \beta_z$ [N/mm]
k_{0j}	Partial derivative of resultant elastic deformation $\delta_{B'_j}$ with respect to the radial displacement $\delta_{x'}$ at $\delta_{Bx'_{0j}}$ in a rotating coordinate system
k_j	Partial derivative of resultant elastic deformation $\delta_{B'_j}$ with respect to the radial displacement $\delta_{x'}$ at λ_j in a rotating coordinate system
l_{eff}	Effective roller length [mm]

*Corresponding author

Email address: gregor.cepon@fs.uni-lj.si (Gregor Čepon)

M_i	Mean bearing moment about $i = x, y, z$ directions [N mm]
\mathbf{m}	Bearing smoothing vector, composed by the user-defined values of deformation μ_{0j} , below which smoothing is applied ($j = 1, 2, \dots, z$)
n	Rolling-element load-deflection exponent
\mathbf{q}_b	Mean bearing displacement vector, composed by the mean bearing translational displacements δ_i and the mean bearing rotational displacements β_i ($i = x, y, z$)
\mathbf{R}	Rotational transformation matrix from fixed to rotating Cartesian coordinate system
r_b	Radius of rolling element in ball bearings [mm]
r_j	Pitch radius (roller) or radii of inner raceway groove's curvature centres (ball) [mm]
r_c	Bearing radial clearance [mm]
z	Total number of rolling elements in a bearing
α_0	Unloaded bearing contact angle [rad]
α_j	Loaded j th rolling element contact angle [rad]
β_i	Mean bearing rotational displacement about the $i = x, y, z$ axis [rad]
δ_{B_j}	Resultant elastic deformation of the j th ball element [mm]
$\delta_{Bx'_{0j}}$	Displacement of the j th ball in a radial direction (x') needed to overcome the clearance [mm]
δ_{R_j}	Resultant elastic deformation of the j th roller element [mm]
$\delta_{Rx'_{0j}}$	Displacement of the j th roller in a radial direction (x') needed to overcome clearance [mm]
$\delta_{T'_j}$	Smoothed resultant elastic deformation of the j th rolling element in a region of contact-state transition [mm]
δ_i	Mean bearing translational displacement in the $i = x, y, z$ direction [mm]
δ_{r_j}	Effective j th rolling element displacement in the radial direction [mm]
δ_{z_j}	Effective j th rolling element displacement in the axial direction [mm]
λ_j	Radial displacement at which a deformation of the j th rolling element is equal to μ_j [mm]
μ_{0j}	User-defined value of deformation of the j th rolling element below which smoothing is applied [mm]
μ_j	Exact value of deformation of the j th rolling element below which a smoothing is applied [mm]
φ	Angle between rotational and fixed coordinate system [rad]
ψ_j	Angular distance of the j th rolling element from the x -axis [rad]
$(\dots)'$	Arbitrary previously defined symbol in rotating coordinate system (x', y', z')

1. Introduction

The dynamic characterization of rolling bearings has been investigated for many decades; however, due to its complexity it remains an important matter in ongoing research. Despite a great increase in computer power in recent years and consequently computer-aided engineering (CAE), the modelling of bearing dynamics continues at the analytical level. These analytically derived dynamic bearing models are afterwards inserted into a numerical model of the system in the sense of a shaft-bearing-housing assembly. Due to the nonlinear nature of the contact formulation in rolling bearings, the prediction of the system's response remains a tedious task.

A first general theory for elastically constrained ball and roller bearings was developed by Jones [1] and later on further derived by Harris [2]. This theory was in fact very general and it was not able to properly determine the cross-coupling stiffness between the radial, axial and the tilting deflections. Simplified bearing models were instead introduced by other researchers, where the bearings were modelled as ideal boundary conditions for the shaft, as presented by Rao [3]. Meanwhile, the idea of interpreting the bearings with a simple one- or two-degrees-of-freedom (DOFs) model with linear springs was introduced by While [4] and Gargiulo [5]. Later, more precise bearing models were derived. A major improvement in predicting the vibration transmission through rolling-element bearings was made by Lim and Singh [6], who derived a model that provides a comprehensive bearing-stiffness matrix. The model is capable of properly describing the nonlinear relation between the load and the deflection, taking into account all 6 DOFs and their interplay. The model of Lim and Singh was the basis for many subsequent investigations. The same authors described the effect of a distributed contact load on a roller bearing's stiffness matrix [7]. Later, Royston and Basdogan [8] introduced a model for predicting the vibration transmission through

self-aligning (spherical) rolling-element bearings. Liew and Lim [9] extended the model of Lim and Singh to analyse the time-varying rolling element bearing characteristics that occur due to the pass of the rolling element. A bearing-stiffness matrix formulation for double row angular contact ball bearings was derived by Gunduz and Singh [10]. Lee and Choi [11] presented an analysis approach where they investigated the speed-dependent ball-bearing stiffness in a flexible rotor with a nonlinear bearing characteristic based on Jones' model. Sheng et al. [12] studied and derived the bearing speed-varying stiffness model. With the development of the finite-element-method (FEM) models, new techniques for calculating the proper bearing dynamics have appeared. Guo and Parker [13] proposed a stiffness matrix calculation for a rolling-element bearing using a finite-element/contact-mechanics model. The authors precisely modelled each integral part of the bearing and implemented a special contact model derived by Vijayakar [14] between the rolling elements and both raceways. Recently, Zhang et al. [15] presented a general model for preload calculation and stiffness analysis for combined angular contact ball bearings.

Many authors have studied the bearing dynamics by analysing a rotor-bearing-housing assembly. Lim and Singh investigated a geared-rotor system [16, 17] and performed a statistical energy analysis [18]. Bai et al. [19] went step further and analysed the acoustic response. They evaluated the radiation noise of the bearing applied to the ceramic motorized spindle based on the sub-source decomposition method. Čermelj and Boltežar [20] presented an indirect approach to investigate the dynamics of a structure with ball bearings. Lately, Razpotnik et al. [21] investigated the vibration transmission in a statically indeterminate system that is supported by bearings. The dynamic behaviour of a system containing bearings where the time response was calculated was presented by Xu and Li [22, 23] for a planar multibody system with multiple deep groove ball-bearing joints. Fonseca et al. [24] studied the influence of unbalance levels on nonlinear dynamics of a rotor-backup rolling bearing system. Wang et al. [25] conducted dynamic modelling of moment wheel assemblies with nonlinear rolling bearing supports. They performed dynamic tests to verify the nonlinear dynamic model. The effect of bearing preload on the modal characteristics of a shaft-bearing assembly was investigated by Gunduz et al. [26]. Similarly, the effect of the axial preload of the ball bearings on the nonlinear dynamic characteristics of a rotor-bearing system was investigated by Bai et al. [27]. It was shown that the bifurcation margins of an unbalanced rotor-bearing system enhance markedly when the axial preload increases and relates to the system's resonance speed.

Predicting the response of a system with rolling bearings often encounters numerical difficulties when a time integration is performed. The problem originates in a sudden contact-state transition, which is governed by the bearing clearance and the nonlinear force- and stiffness-displacement characteristics. Several attempts have been made to increase the stability of the calculation. Fleming and Poplawski [28] showed that a moderate amount of damping eliminated the bistable region in their response, but this damping is not inherent in the ball bearings and introduces additional artificial forces. Another approach was presented by Xia et al. [29] for the rotor-bearing system with journal bearings. They presented two calculation methods (the Ritz model and a one-dimensional FEM) to overcome the numerical shortcomings of the extremely time-consuming Reynolds equations.

In this paper a new formulation for the contact-state transition is presented for rolling-element bearings with a radial clearance to ensure a stable numerical calculation. The original non-smooth contact-dynamics formulation implies numerical issues in a time-integration process. In order to avoid these problems the proposed formulation introduces smooth bearing deformation-displacement characteristics in the region of the impact contacts. The idea is somehow similar to the modelling of a non-smooth friction force using an approximate single-valued friction law [30]. The bearing model from Lim and Singh [6] represents the basis for our study. Since the formulation proposes the smoothing of deformations, the whole existing bearing model has to be reformulated and new equations have to be derived to obtain a comprehensive bearing-stiffness matrix. The modularity of the proposed bearing model allows the implementation of an arbitrary smoothing value for each individual rolling element. The applicability of the newly developed bearing model is demonstrated on a simple unbalanced rotor that is supported by two bearings. It is shown that already a small value of the smoothing parameter significantly improves the numerical simulation in terms of speed and stability. The aim of the presented work is not to change the bearing design, but to facilitate the calculation process. Many engineering applications related to the rotating machinery might find the presented contribution valuable.

2. Assumptions

Besides the assumptions given in [6] the following also have to be taken into account:

1. The radial load is dominant.
2. It is applicable to bearings that operate under a radial clearance. Therefore, ball and cylindrical roller bearings are of primary interest.
3. The new, rotating coordinate system is used, which follows the direction of the radial load. Radial x -axis points directly to one rolling element (as assumed already in [6]). Consequently, any fluctuation due to a rolling-element pass is neglected.

3. The existing analytical bearing model

3.1. Presentation of the 6-DOFs bearing model

Having the bearing mean-load vector $\mathbf{f}_b = \{F_x, F_y, F_z, M_x, M_y, M_z\}^T$ and the bearing mean-displacement vector $\mathbf{q}_b = \{\delta_x, \delta_y, \delta_z, \beta_x, \beta_y, \beta_z\}^T$ as shown in Fig. 1, we can express the radial and axial displacements of

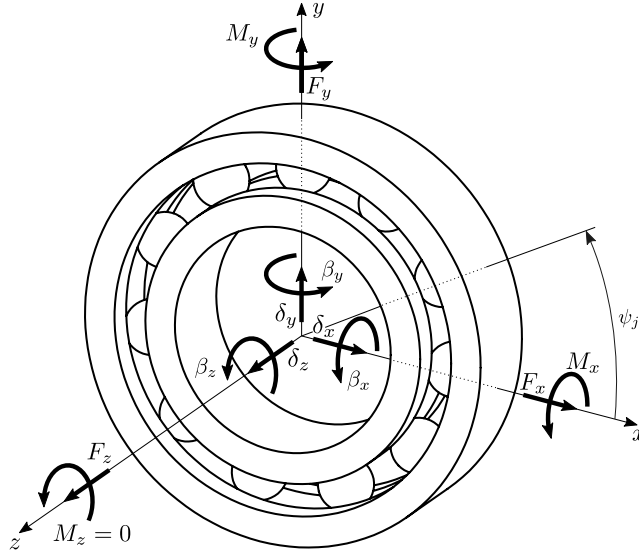


Figure 1: Rolling-element bearing loads and displacements.

the j th rolling element as

$$\delta_{r_j} = \delta_x \cos \psi_j + \delta_y \sin \psi_j - r_c \quad (1)$$

and

$$\delta_{z_j} = \delta_z + r_j(\beta_x \sin \psi_j - \beta_y \cos \psi_j), \quad (2)$$

where x and y point to the radial direction and z to the axial direction (Cartesian coordinate system). The moment around z -axis is zero by default (no friction). For ball bearings the contact angle of the j th ball is defined as $\tan \alpha_j = \frac{\delta_{z_j}^*}{\delta_{r_j}^*}$, where $\delta_{z_j}^* = A_0 \sin \alpha_0 + \delta_{z_j}$ and $\delta_{r_j}^* = A_0 \cos \alpha_0 + \delta_{r_j}$, as shown in Fig. (2). For cylindrical roller bearings it is assumed that $\alpha_j = \alpha_0 = 0$. The loaded distance between the inner- and outer-raceway curvature centres for the j th ball is given as:

$$A(\psi_j) = A_j = \sqrt{(\delta_{r_j}^*)^2 + (\delta_{z_j}^*)^2}. \quad (3)$$

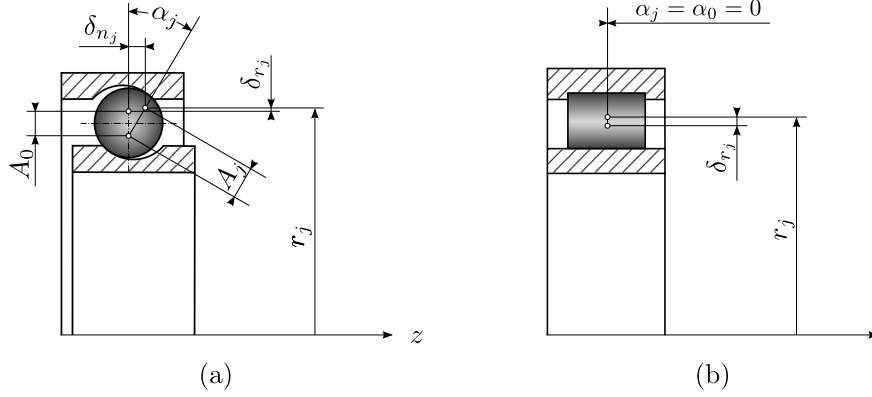


Figure 2: Elastic deformation of rolling element; (a) Non-constant contact angle α_j , (b) Constant contact angle $\alpha_j = \alpha_0$.

From the ball-bearing kinematics, the resultant elastic deformation of the j th ball is defined as:

$$\delta_{B_j} = \begin{cases} A_j - A_0, & \delta_{B_j} > 0 \\ 0, & \delta_{B_j} \leq 0 \end{cases}, \quad (4)$$

whereas for cylindrical roller bearings, the resultant elastic deformation of the j th roller is equal to:

$$\delta_{R_j} = \begin{cases} \delta_{r_j}, & \delta_{R_j} > 0 \\ 0, & \delta_{R_j} \leq 0 \end{cases}. \quad (5)$$

Following the Hertzian contact stress principle as $F_j = K_n \delta_j^n$ (n is equal to $3/2$ for ball bearings and $10/9$ for roller bearings), we can connect \mathbf{f}_b and \mathbf{q}_b by summing the contribution from the rolling elements:

$$\mathbf{f}_b = \begin{Bmatrix} F_x \\ F_y \\ F_z \\ M_x \\ M_y \end{Bmatrix} = \begin{Bmatrix} \sum_{j=1}^z F_j \cos \alpha_j \cos \psi_j \\ \sum_{j=1}^z F_j \cos \alpha_j \sin \psi_j \\ \sum_{j=1}^z F_j \sin \alpha_j \\ \sum_{j=1}^z r_j F_j \sin \alpha_j \sin \psi_j \\ - \sum_{j=1}^z r_j F_j \sin \alpha_j \cos \psi_j \end{Bmatrix}, \quad (6)$$

where z is the number of all the rolling elements in a bearing. Finally, the symmetrical bearing-stiffness matrix with dimension five is expressed as:

$$\mathbf{K}_b = \frac{\partial \mathbf{f}_b}{\partial \mathbf{q}_b} = \begin{bmatrix} k_{xx} & k_{xy} & k_{xz} & k_{x\beta_x} & k_{x\beta_y} \\ & k_{yy} & k_{yz} & k_{y\beta_x} & k_{y\beta_y} \\ & & k_{zz} & k_{z\beta_x} & k_{z\beta_y} \\ \text{sym.} & & & k_{\beta_x\beta_x} & k_{\beta_x\beta_y} \\ & & & & k_{\beta_y\beta_y} \end{bmatrix}. \quad (7)$$

It is important to note that \mathbf{K}_b is symmetrical and in general with dimension 6×6 ; however, due to the zero stiffness terms connected with β_z we obtain a matrix with a rank of five.

3.2. The origin of the numerical problems in the explicit calculations

The bearing model presented in Section 3.1 is of great use in all kinds of implicit calculations. However, when it comes to explicit dynamics – using either the Finite Element Method (FEM) model or Multi-Body Simulations (MBS) – some numerical difficulties arise due to the bearing clearance.

For the sake of clarity, let us present an example. The ball and cylindrical roller bearings, with properties as given in Table 2, are subjected to a pure radial displacement in the x direction. The implied displacement

Table 2: Properties of both bearings for the given example.

type	d [mm]	D [mm]	r_c [μm]	z	r_b [mm]	l_{eff} [mm]
ball	30	72	20	8	6	/
roller	30	72	20	8	/	11

results in the deformation of some rolling elements. Due to the clearance, there is a gap between the rolling element and the inner/outer ring (Fig. 3). It can be seen that the deformation of the j th rolling element is the same for the ball and roller types. It is reasonable that this applies only to the bearings with the same main geometry (Table 2). However, the stiffness characteristics in the corresponding radial direction change significantly between both types of bearing, due to the different contact types, i.e., point/line contact. The stiffness characteristics of both bearing types are continuous functions, but are not also continuously differentiable. Additionally, the discontinuity of the stiffness derivative is not significant only in the region where the clearance is exceeded, but also in the areas where the neighbouring rolling elements gradually come into contact.

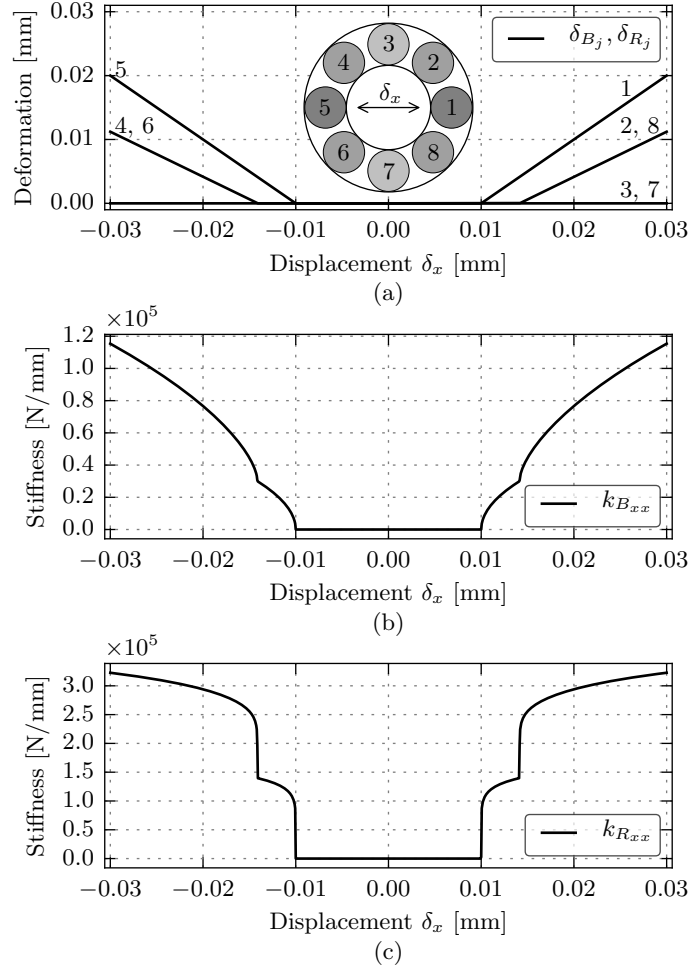


Figure 3: Deformation and radial stiffness characteristics of bearings; (a) Deformation, (b) Stiffness of ball bearing, (c) Stiffness of cylindrical roller bearing.

When running explicit calculations it is important to have a system whose integral parts exhibit con-

tinuously differentiable stiffness-displacement characteristics. Otherwise, a time step during the integration process decreases significantly, which results in a longer computational time or even leads to non-converged solutions. A similar problem is well known in contact mechanics when modelling a friction phenomenon.

4. Smoothing the contact-state transition

A contact change from open to closed represents a transient phenomenon. When the transition is very fast in terms of time, we can talk about impacts. They change the dynamic properties of a system significantly in a very short time. In the case of bearings, this happens when the rolling elements eliminate the clearance and suddenly hit the raceways. This sudden change of the bearing load vector and the corresponding bearing stiffness represents the root cause of many problems in a time-integration procedure.

An efficient way to improve the calculation of a system with a sudden contact-state transition is to derive the smoothed force and the corresponding stiffness characteristics in the area of the transition. A sudden hit, which appears every time each single rolling element eliminates the clearance and hits between both raceways can be effectively smoothed. The transition is especially problematic for the first rolling element coming into a contact (Fig. 3). The smooth contact transition introduces “simplification”, which helps the integration process to pass that region flawlessly. Smoothing a function implies an approximate final solution in the region where the smoothing is applied. Obviously, there is a trade-off between the exact solution with numerical difficulties and the approximate one with numerical ease.

4.1. Theoretical background

A sudden transition of the force- and stiffness-displacement characteristics originates in piecewise-defined ball- and roller-bearing kinematics as given in Eq. (4) and (5). Thus, it is reasonable to smooth the function regulation in the region between both pieces. Furthermore, this change is to be conducted on the deformation level so that the derived expressions for the force- and stiffness-displacement characteristics are to be smoothed as well. From Eq. (4) and (5) it follows that

$$A_j - A_0 = 0 \quad \text{and} \quad \delta_{r_j} = 0 \quad (8)$$

represent the points between both function intervals of the j th rolling element for a ball and cylindrical roller bearing, respectively. Since radial load is dominant and most sensitive to the impacts, we have to find the roots of Eq. (8) in radial (x') direction. The roots represent the radial displacement of each j th rolling element (as a function of all other DOFs), needed to overcome a clearance. First, we define a new rotating Cartesian coordinate system as shown in Fig. 4. The axes z' and z are aligned, whereas the axes x' and y' rotate around z' . Such a coordinate system enables the definition of a radial displacement entirely in the $x'z'$ plane, having a displacement in the y' direction always equal to zero. The new mean-load and mean-displacement vectors are defined as:

$$\begin{aligned} \mathbf{f}_{b'} &= \{F_{x'}, F_{y'} = 0, F_{z'}, M_{x'}, M_{y'}, M_{z'} = 0\}^T, \\ \mathbf{q}_{b'} &= \{\delta_{x'}, \delta_{y'} = 0, \delta_{z'}, \beta_{x'}, \beta_{y'}, \beta_{z'}\}^T. \end{aligned} \quad (9)$$

The transformation from the fixed to the rotating coordinate system is equal to

$$\mathbf{q}_{b'} = \mathbf{R} \mathbf{q}_b, \quad (10)$$

where \mathbf{R} is a rotational transformation matrix. Hereinafter, all the parameters and properties that refer to the rotating coordinate system are denoted as $(...)'$.

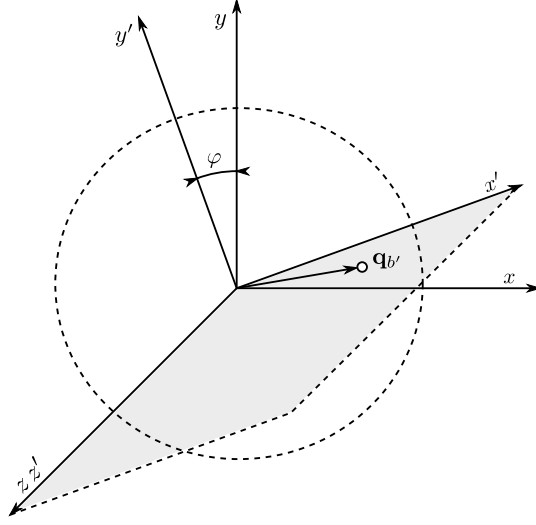


Figure 4: Fixed and rotating coordinate systems.

4.1.1. Ball bearings

By transforming Eq. (8) to the rotating coordinate system we can express the roots of Eq. (8) in x' direction as a function of all other displacements and rotations:

$$\begin{aligned}
 A_{j'} - A_0 &= 0 \\
 (A_0 \cos \alpha_0 + \delta_{x'} \cos \psi'_j - r_c)^2 &= (A_0^2 - (\delta_{z'_j}^*)^2) \\
 \delta_{x'_{B0j}} &= \frac{1}{\cos \psi'_j} \left(r_c - A_0 \cos \alpha_0 + \sqrt{A_0^2 - (\delta_{z'_j}^*)^2} \right)
 \end{aligned} \tag{11}$$

Having an arbitrary $\mathbf{q}_{b'}$, Eq. (11) gives the exact radial displacement $\delta_{x'_{B0j}}$ at which every j th ball is coming into contact. Going back to Eq. (4) with all the radial roots $\delta_{x'_{B0j}}$ known, we have to make the transition smooth. In order to achieve that, the value of the deformation $\delta_{B'_j}$ below which the smoothing is to be applied has to be defined. This value is initially given by the user and we denote it as μ_{0j} . If $\delta_{B'_j}$ is a linear function (valid only when all the other than radial displacement are equal to zero), we calculate the corresponding radial displacement as:

$$\lambda_j = \delta_{x'_{B0j}} + \frac{\mu_{0j}}{k_{0j}}, \tag{12}$$

where k_{0j} is the slope of $\delta_{B'_j}$ at $\delta_{x'_{B0j}}$. However, in general $\delta_{B'_j}$ is not linear (Eq. (3)) and the slope in the radial direction is a function of $\mathbf{q}_{b'}$, which can be expressed as:

$$k_j = k_j(\mathbf{q}_{b'}) = \frac{\partial \delta_{B'_j}}{\partial x'} = \frac{\delta_{r'_j}^*}{A'_j} \cos \psi'_j. \tag{13}$$

Thus, an exact deformation μ_j , which is equal to $\delta_{B'_j}(\lambda_j)$ differs slightly from μ_{0j} , as demonstrated in Fig. 5. Based on the initial μ_{0j} we can calculate the parameters λ_j , μ_j and k_j , which are crucial to define a smoothing function. For the latter we use a hyperbolic tangent function of the form:

$$\delta_{T'_j} = \mu_j \left(\tanh \left(\frac{k_j}{\mu_j} (\delta_{x'} - \lambda_j) \right) + 1 \right). \tag{14}$$

Fig. 6 shows $\delta_{B'_j}$ and $\delta_{T'_j}$ as a function of the radial displacement $\delta_{x'}$ (other displacements and rotations are here equal to zero). It is clear that a combination of the functions $\delta_{B'_j}$ and $\delta_{T'_j}$ results in a continuously differentiable function, since their values and derivatives at λ_j are exactly the same.

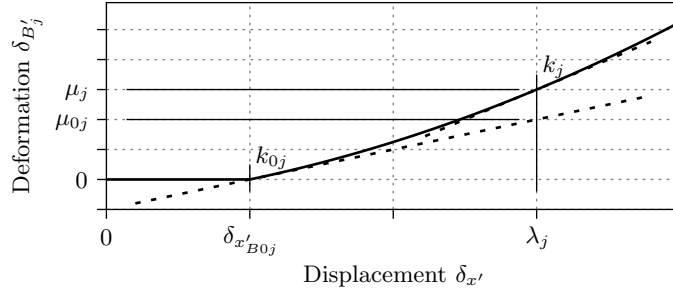


Figure 5: The parameters of the smoothing algorithm.

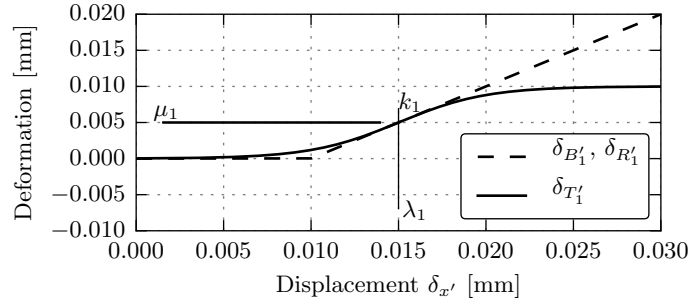


Figure 6: Resultant elastic deformation and corresponding smoothing function for the 1st rolling element.

4.1.2. Cylindrical roller bearings

Analogously to the derivation of the roots in the radial direction for ball bearings, we can write the roots of Eq. (8) for cylindrical roller bearings as:

$$\begin{aligned} \delta_{r'_j} &= 0 \\ \delta_{x'_{R0j}} &= \frac{r_c}{\cos \psi'_j} \end{aligned} \quad (15)$$

Concerning the cylindrical roller bearings, loads other than radial loads are negligible [6]. Therefore, $\delta_{R'_j}$ can be treated as a linear function of the radial displacement $\delta_{x'}$. So like for ball bearings we define:

$$\lambda_j = \delta_{x'_{R0j}} + \frac{\mu_{0j}}{k_{0j}}, \quad (16)$$

where $\mu_{0j} = \mu_j$ and $k_{0j} = k_j$ due to the linear δ_{R_j} characteristics for cylindrical roller bearings. The slope of $\delta_{R'_j}$ is equal to:

$$k_j = \frac{\partial \delta_{R'_j}}{\partial x'} = \cos \psi'_j. \quad (17)$$

By knowing all the necessary parameters (λ_j, μ_j, k_j) we use a smoothing function of the form given in Eq. (14). Consequently, the deformation characteristics are smoothed as shown in Fig. 6.

4.2. Application of the smoothing algorithm to the existing bearing model

The idea of smoothing piecewise-defined bearing kinematics is applied to the well-established bearing model of Lim and Singh [6].

4.2.1. Ball bearings

The resulting elastic deformation of the j th ball is redefined as:

$$\delta_{B'_j} = \begin{cases} A'_j - A_0, & \delta_{B'_j} > \mu_j \\ \mu_j \left(\tanh \left(\frac{k_j}{\mu_j} (\delta_{x'} - \lambda_j) \right) + 1 \right), & \delta_{B'_j} \leq \mu_j \end{cases}. \quad (18)$$

It is important to note that $\delta_{B'_j}$ in Eq. (18) cannot be smaller than zero, since the defined hyperbolic tangent function asymptotically approaches zero. Additionally, a radial displacement $\delta_{x'}$ is never negative due to the definition of the rotating coordinate system. Taking into account that $\cos \alpha_j = \frac{\delta_{r'_j}^*}{A'_j}$ [6] we can write the force in the radial direction as:

$$F_{x'} = K_n \sum_{j=1}^z \delta_{B'_j}^n \frac{\delta_{r'_j}^*}{A'_j} \cos \psi'_j. \quad (19)$$

By inserting Eq. (18) into Eq. (19) we obtain:

$$F_{x'} = K_n \sum_{j=1}^z \frac{\delta_{r'_j}^*}{A'_j} \cos \psi'_j \begin{cases} (A'_j - A_0)^n, & \delta_{B'_j} > \mu_j \\ \left(\mu_j \left(\tanh \left(\frac{k_j}{\mu_j} (\delta_{x'} - \lambda_j) \right) + 1 \right) \right)^n, & \delta_{B'_j} \leq \mu_j \end{cases}. \quad (20)$$

Other elements of the load vector $\mathbf{f}_{b'}$ retain the original form (except $F_{y'} = 0$ as defined in Eq (9)). The stiffness in the radial direction is further derived as:

$$k_{B'_{xx}} = K_n \sum_{j=1}^z \left(\frac{\partial}{\partial x'} \left(\delta_{B'_j}^n \right) \frac{\delta_{r'_j}^*}{A'_j} + \delta_{B'_j}^n \frac{\partial}{\partial x'} \left(\frac{\delta_{r'_j}^*}{A'_j} \right) \right) \cos \psi'_j. \quad (21)$$

Due to the piecewise definition of $\delta_{B'_j}$, Eq. (21) has the form:

$$k_{B'_{xx}} = K_n \sum_{j=1}^z \begin{cases} P_{Bi}, & \delta_{B'_j} > \mu_j \\ R_{Bi}, & \delta_{B'_j} \leq \mu_j \end{cases}, \quad (22)$$

where

$$P_{Bi} = \frac{1}{(A'_j)^3} (A'_j - A_0)^n \cos^2 \psi'_j \cdot \left(\frac{n A'_j (\delta_{r'_j}^*)^2}{A'_j - A_0} + (A'_j)^2 - (\delta_{r'_j}^*)^2 \right) \quad (23)$$

and

$$R_{Bi} = \delta_{B'_j}^n \left(\frac{n k_j \delta_{r'_j}^*}{\delta_{B'_j} A'_j} \left(1 - \tanh^2 \left(\frac{k_j}{\mu_j} (\delta_{x'} - \lambda_j) \right) \right) + \frac{(\delta_{r'_j}^*)^2}{(A'_j)^3} \cos \psi'_j \right) \cos \psi'_j. \quad (24)$$

When $\delta_{B'_j} > \mu_j$, Eq. (22) yields the same expression as in the existing 6-DOFs model [6]. However, when $\delta_{B'_j} \leq \mu_j$, a new, smooth force and stiffness characteristic is utilized.

4.2.2. Cylindrical roller bearings

Similarly to the ball bearings, the resultant elastic deformation of the j th roller is redefined as:

$$\delta_{R'_j} = \begin{cases} \delta_{x'} \cos \psi'_j - r_c, & \delta_{R'_j} > \mu_j \\ \mu_j \left(\tanh \left(\frac{k_j}{\mu_j} (\delta_{x'} - \lambda_j) \right) + 1 \right), & \delta_{R'_j} \leq \mu_j \end{cases}. \quad (25)$$

The force in the radial direction can be expressed as:

$$F_{x'} = K_n \sum_{j=1}^z \delta_{R'_j}^n \cos \psi'_j. \quad (26)$$

After considering Eq. (25) we obtain:

$$F_{x'} = K_n \sum_{j=1}^z \cos \psi'_j \cdot \begin{cases} (\delta_{x'} \cos \psi'_j - r_c)^n, & \delta_{R'_j} > \mu_j \\ \left(\mu_j \left(\tanh \left(\frac{k_j}{\mu_j} (\delta_{x'} - \lambda_j) \right) + 1 \right) \right)^n, & \delta_{R'_j} \leq \mu_j \end{cases} . \quad (27)$$

So like in the ball-bearing formulation, the other elements of the load vector \mathbf{f}_b' retain their original form. The radial stiffness term transforms to:

$$k_{R'_{xx}} = K_n \sum_{j=1}^z \left(\frac{\partial}{\partial x'} \left(\delta_{R'_j}^n \right) \cos \psi'_j \right) . \quad (28)$$

By inserting Eq. (25) into Eq. (28) we obtain the following expression:

$$k_{R'_{xx}} = K_n \sum_{j=1}^z \begin{cases} P_{Ri}, & \delta_{R'_j} > \mu_j \\ R_{Ri}, & \delta_{R'_j} \leq \mu_j \end{cases} , \quad (29)$$

where

$$P_{Ri} = n \delta_{R'_j}^{n-1} \cos^2 \psi'_j \quad (30)$$

and

$$R_{Ri} = k_j \delta_{R'_j}^{n-1} \left(1 - \tanh^2 \left(\frac{k_j}{\mu_j} (\delta_{x'} - \lambda_j) \right) \right) \cos \psi'_j \quad (31)$$

Again, when $\delta_{R'_j} > \mu_j$, Eq. (29) yields the same expression as in the existing 6-DOFs model for the cylindrical roller bearings [6]. Additionally, when $\delta_{R'_j} \leq \mu_j$, a smooth stiffness characteristic is obtained.

The proposed model introduces a smooth transition between the open- and the closed-contact states in the radial direction. Initially, it is necessary to specify the level of deformation μ_{0j} (for every j th rolling element), below which the smoothing is applied. All the μ_{0j} are joined together in a bearing-smoothing vector as:

$$\mathbf{m} = \{\mu_{01}, \mu_{02} \dots \mu_{0z}\}^T . \quad (32)$$

It is important to note that the first element in \mathbf{m} represents the first rolling element coming into contact. If the smoothing vector \mathbf{m} contains zeros only, no smoothing is applied and the theory yields the formulation of the existing 6-DOFs model.

4.3. Comparison between the existing and the proposed bearing models

Ball and cylindrical roller bearings (Table 2) are investigated. Fig. 7 shows the deformation as a function of the radial displacement. The characteristics for the ball and the cylindrical roller bearings are identical due

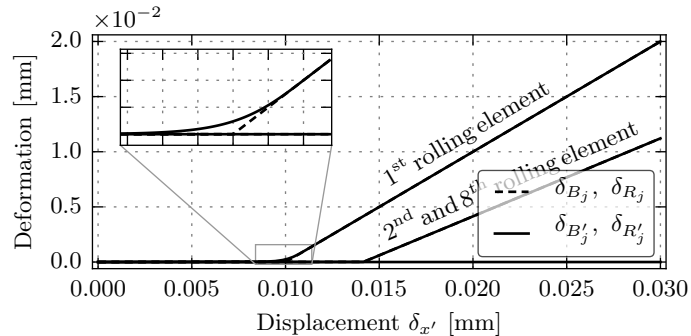


Figure 7: Comparison of deformations between existing and proposed bearing models ($\mu_{01} = 1 \mu\text{m}$).

to them having the same main geometry. As seen from the zoomed-in region, the smoothing is applied to the

first rolling element coming into contact ($\mu_{01} = 1 \mu\text{m}$). The other rolling elements are left without smoothing. Such a smoothed deformation characteristic leads to the modified force- and stiffness-displacement relations, as shown in Fig. 8 and Fig. 9 for ball and cylindrical roller bearings, respectively. It is already clear that a small value of smoothing, e.g., $1 \mu\text{m}$, causes a significant change in the force and stiffness characteristics. The change is even more noticeable for the cylindrical roller bearings. The smoothing reflects in the region

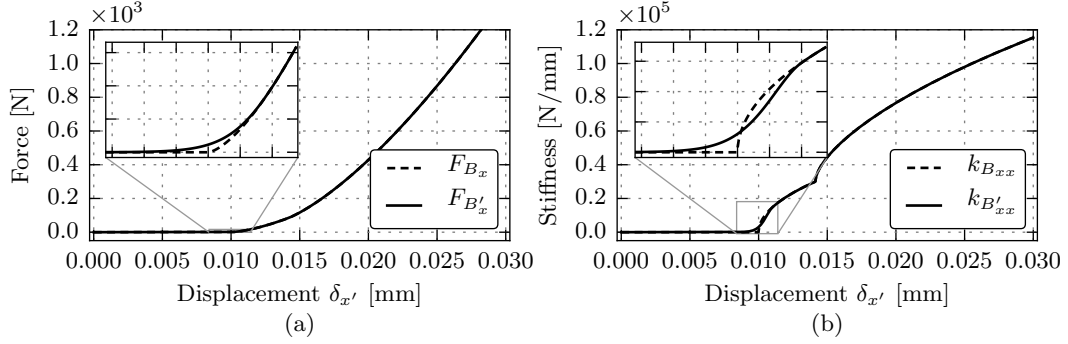


Figure 8: Existing and proposed ball-bearing models ($\mu_{01} = 1 \mu\text{m}$); (a) Force-displacement characteristic, (b) Stiffness-displacement characteristic.

where the first rolling element comes into contact, since only $\mu_{01} = 1 \mu\text{m}$ and other elements are equal to zero.

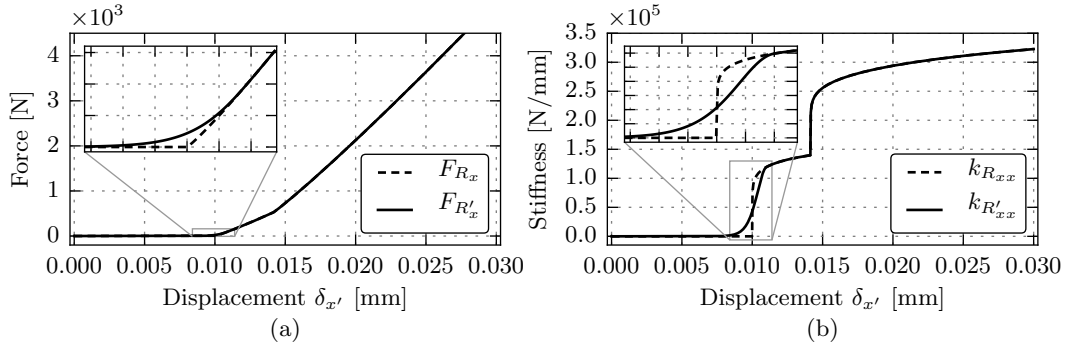


Figure 9: Existing and proposed cylindrical roller bearing models ($\mu_{01} = 1 \mu\text{m}$); (a) Force-displacement characteristic, (b) Stiffness-displacement characteristic.

Ball bearings in comparison to the cylindrical roller ones express additional dependency on the other degrees of freedom. For instance, if a ball bearing is already a little axially displaced, but still within the clearance area, a smaller radial displacement will cause an impact as in the case where there is no axial displacement. Fig. 10 illustrates the phenomenon, presenting an interplay of the axial and radial displacements on the radial stiffness. The characteristics before and after the smoothing are shown. Like with the axial displacement, also the rotational degrees of freedom influence the nature of the contact state. Fig. 11 illustrates the influence of the rotation $\beta_{x'}$ and the radial displacement $\delta_{x'}$ on the overall radial stiffness of the bearings. Furthermore, Fig. 12 shows the effect of the rotation $\beta_{y'}$ and the radial displacement $\delta_{x'}$ on the bearing's radial stiffness. The applied smoothing vector \mathbf{m} for all three combinations contains the elements as follows: $\mu_{01} = 2 \mu\text{m}$ and $\mu_{0j} = 1 \mu\text{m}$, $j = 2, 3 \dots 8$. The effect of the smoothing is clearly shown in all the transitions where a certain ball is coming or leaving the contact. The proposed analytical bearing model has a modular nature, i.e., every single adjustment can be achieved with smoothing vector \mathbf{m} .

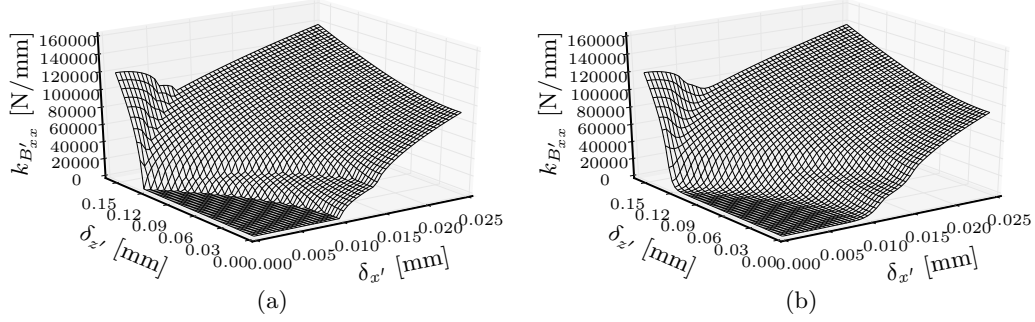


Figure 10: Radial stiffness vs. radial and axial displacements of a ball bearing; (a) Existing model, (b) Proposed model with $\mu_{01} = 2 \mu\text{m}$ and $\mu_{0j} = 1 \mu\text{m}$, $j = 2, 3 \dots 8$.

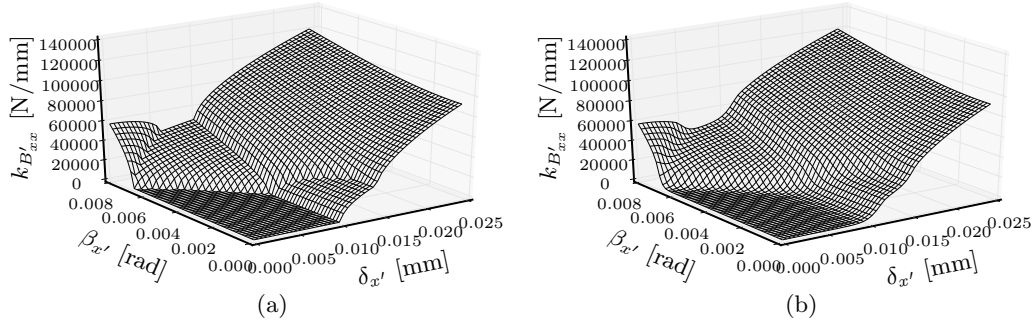


Figure 11: Radial stiffness vs. radial displacement and rotation around the x' -axis of a ball bearing; (a) Existing model, (b) Proposed model with $\mu_{01} = 2 \mu\text{m}$ and $\mu_{0j} = 1 \mu\text{m}$, $j = 2, 3 \dots 8$.

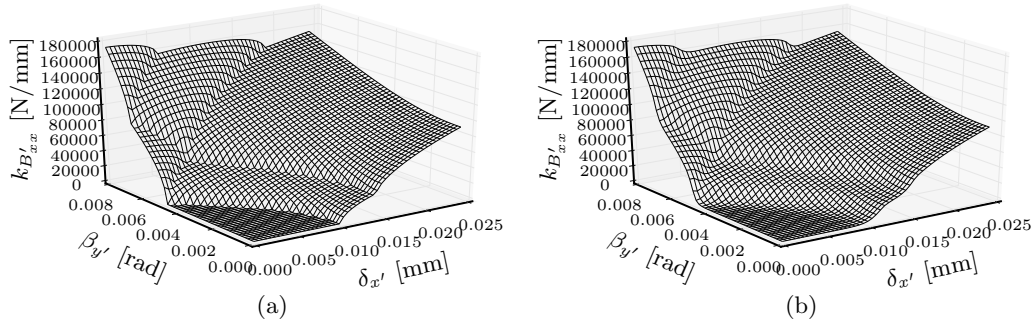


Figure 12: Radial stiffness vs. radial displacement and rotation around the y' -axis of a ball bearing; (a) Existing model, (b) Proposed model with $\mu_{01} = 2 \mu\text{m}$ and $\mu_{0j} = 1 \mu\text{m}$, $j = 2, 3 \dots 8$.

5. Case study

The applicability of the proposed bearing model is presented in a case study. The simple FEM model assembly (Fig. 13) consists of a shaft, two different bearings (ball and cylindrical roller) and a housing, connected to the rigid base. Two separate masses simulate the dynamic load. The geometrical parameters of the bearings are given in Table 3. The inner and outer rings of both bearings are modelled with conventional FEM solid elements, whereas the rolling elements are not modelled, but incorporated into the bearing-stiffness matrix. Both raceways are connected into two separate central nodes. The analytically calculated

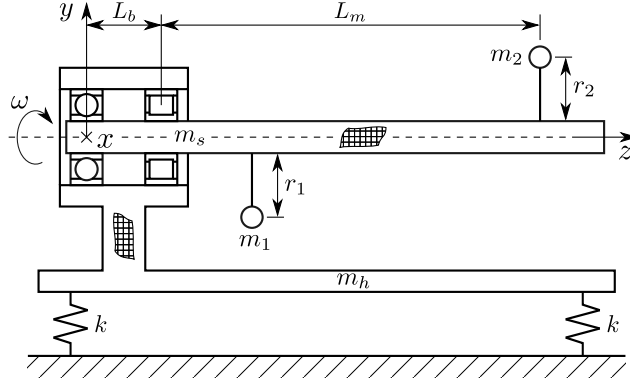


Figure 13: Schematically presented FEM model assembly used for the case study.

Table 3: Properties of the ball and cylindrical roller bearings for the presented case study.

type	code	d [mm]	D [mm]	r_c [μm]	z	r_b [mm]	l_{eff} [mm]
ball	6306	30	72	20	8	6	/
roler	N306	30	72	45	12	/	11

nonlinear bearing-stiffness matrix is prescribed between both central nodes, as demonstrated in Fig. 14. The

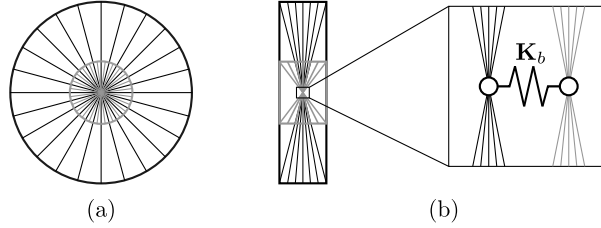


Figure 14: A bearing in the FEM model (black – outer ring, grey – inner ring); (a) Spider elements connecting both raceways, (b) Bearing-stiffness matrix prescribed between the central nodes.

geometrical and material properties of the assembly are given in Table 4. Furthermore the mass moments of inertia are given in Table 5.

Table 4: Geometrical and material properties for the FEM model.

m_s [kg]	m_h [kg]	m_1 [kg]	m_2 [kg]	r_1 [mm]	r_2 [mm]	L_b [mm]	L_m [mm]	k [N/mm]
18.0	34.4	0.1	0.05	241	241	100	356	9

Table 5: Mass moments of inertia for the FEM model.

	I_{xx} [kg mm ²]	I_{yy} [kg mm ²]	I_{zz} [kg mm ²]	I_{xy} [kg mm ²]	I_{yz} [kg mm ²]	I_{zx} [kg mm ²]
shaft	703867	703840	891556	0	-3085	0
housing	3305360	1426527	3076361	346075	952903	136095

The aim of our case study is to present the time response during the system's run-up. The shaft (and eccentric masses), together with both bearing's inner rings and associated spider elements rotate by

prescribed movement. In every time step the displacements and rotations between both central nodes of each bearing are calculated (displacement vector \mathbf{q}_b). Based on \mathbf{q}_b the bearing stiffness is provided. The original and the proposed bearing models are utilized. For the latter we prescribe $\mu_{01} = 2 \mu\text{m}$, whereas the other elements of the smoothing vector are equal to zero. It is important to note that μ_{01} has, in general, the greatest influence on the performance of the calculation. The shaft is governed by a constant angular acceleration $\dot{\omega} = 0.8 \text{ rev/s}^2$, starting with $\omega = 0$. The damping ratio used in the FEM model is equal to 0.1 and the numerical method employed for the time integration is Runge-Kutta-Fehlberg. Two different regions will be presented, i.e., the initial stage of run-up and the region near the system's resonance.

5.1. Initial stage of run-up

The initial stage of run-up represents the first 8 seconds of the simulation. It is important to define the initial conditions, i.e., both bearings have their inner and outer rings concentrically aligned and the shaft is not rotating. When the simulation starts, the inner rings of both bearings move towards the rolling elements due to gravity and eliminate the clearance (the rolling elements collide with both raceways). At the same time the shaft is subjected to a constant angular acceleration. The radial response $\delta_{x'}$ is shown in Fig. 15 for both bearings. It is clear that the results obtained with the proposed bearing model exhibit a much

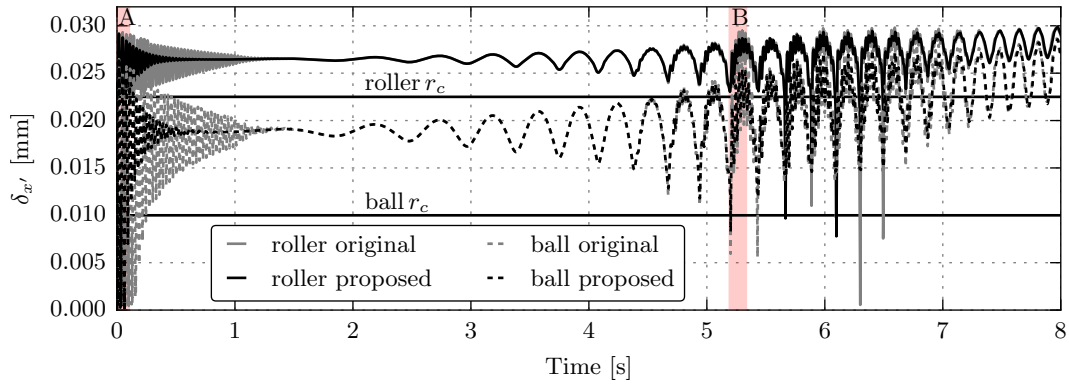


Figure 15: Radial response of both bearings for the original and the proposed bearing model.

more attenuated response. The effect is especially significant in the first second of the simulation, when the shaft reaches the equilibrium position. A small oscillations in the original bearing model appear due to numerical issues, i.e., a high contact force and a stiffness change in a very short time. Two sections, A and B (Fig. 15), are shown separately in Fig 16. The areas A and B reveal details of how the proposed bearing model follows the general behaviour of the original bearing model. Additionally, the power spectral density (PSD) of a time response is presented in a Campbell diagram in Fig. 17 and Fig. 18 for ball and cylindrical type, respectively. The comparison between responses of the original and proposed bearing models is given. It can be seen, that level of higher frequencies is reduced due to the smooth contact initiation. However, the general response remains the same.

Besides the response in a time and frequency domain, the orbital motion of both bearings is also shown in Fig. 19 and Fig. 20. Both figures consist of orbits obtained using the original bearing formulation as well as with the proposed one. The clearance of the bearing is marked as a grey circle in the centre. The attenuated response is also clearly seen in the orbital motion, especially for the ball bearing at the beginning of the simulation. After both bearings reach their equilibrium positions they enter into another region, where a sudden hit from one side to another occurs. This happens since the centrifugal force of the rotating shaft at a certain speed is not yet high enough to push both bearings to the side completely. The region expresses unstable movement of the inner ring with respect to the outer ring. After the angular velocity and, consequently, the centrifugal force are high enough, the inner ring starts to rotate together with the shaft. It is clear that the smoothed bearing model does not provide exactly the same orbits as the original one; however, the motion, in general, is the same.

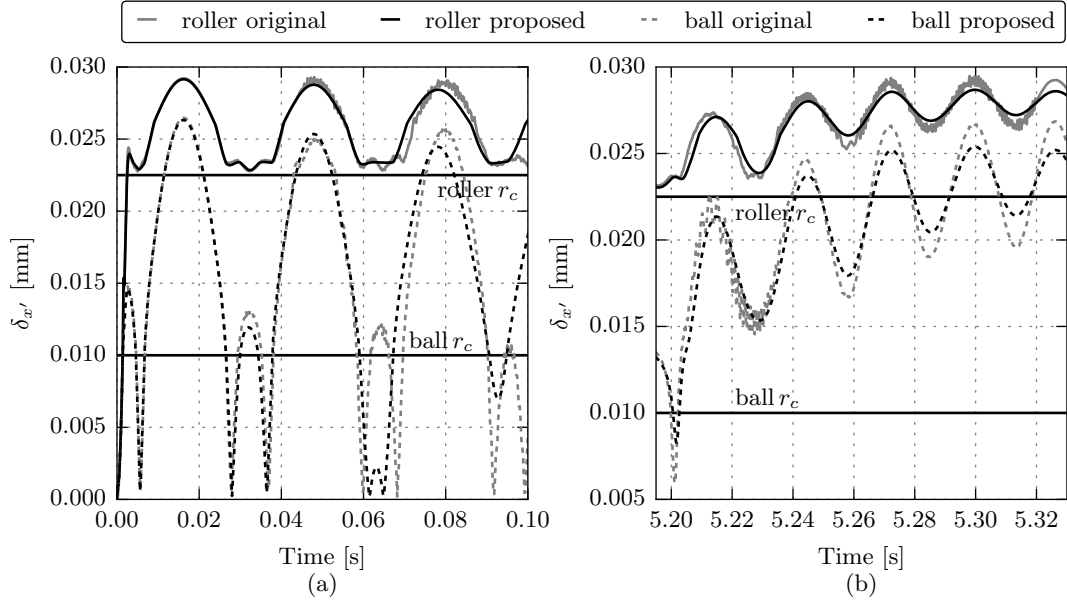


Figure 16: Radial response of both bearings for the original and the proposed bearing model; (a) Region A, (b) Region B.

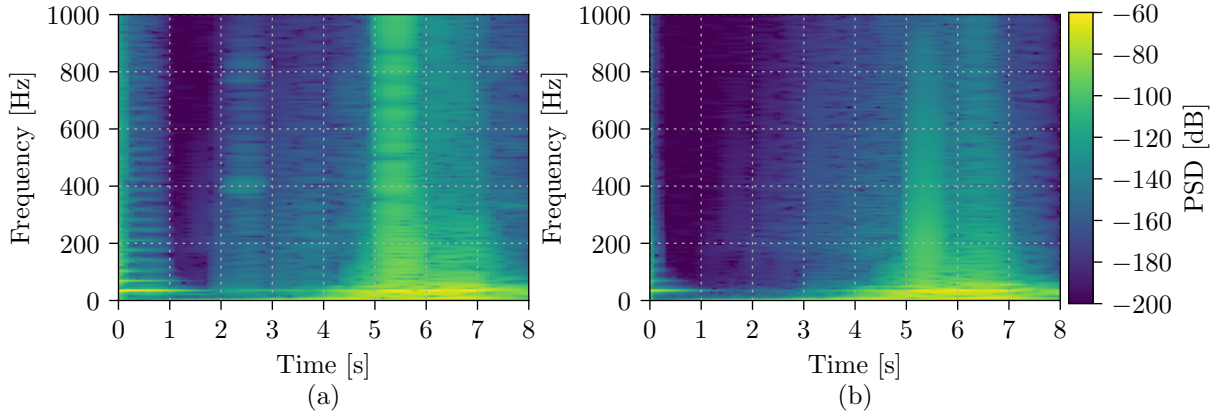


Figure 17: Campbell diagram of the radial response $\delta_{x'}$ for the ball bearing; (a) The original bearing model, (b) The proposed bearing model.

One of the main advantages of the proposed bearing model is a reduction in the computational time. Fig. 21 shows the comparison of the computational times for the first 8 seconds at different smoothing levels. The presented case study with $\mu_{01} = 2 \mu\text{m}$ reduced the computational time by up to 40 % compared to the original bearing model. Employing a smoothing value only helps to a certain extent. Small smoothing values leverage a time-integration process, since they help to avoid numerical issues in the contact-state transition of the bearing. On the other hand, larger smoothing values do not contribute any further to a reduction in the computational time.

5.2. Response near to the system resonance

The proposed bearing model does not only facilitate a time integration in the initial stage of run-up, but also in the region close to the system's resonance. A slightly modified case study is used in order to obtain a representative scenario. A modification in terms of different eccentric masses was made. The new masses are equal to $m_1 = 0.5 \text{ kg}$ and $m_2 = 0.1 \text{ kg}$. Fig. 22 shows the time response of a radial displacement

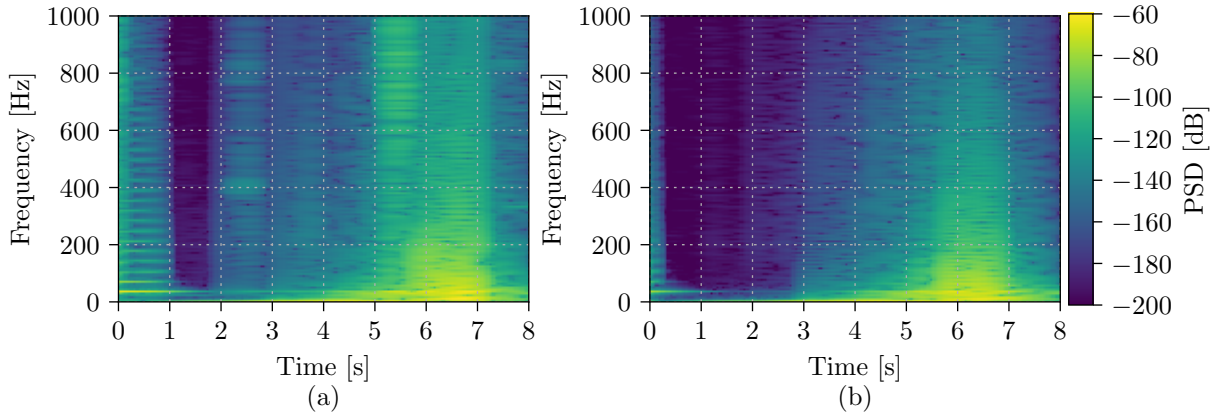


Figure 18: Campbell diagram of the radial response $\delta_{x'}$ for the cylindrical roller bearing; (a) The original bearing model, (b) The proposed bearing model.

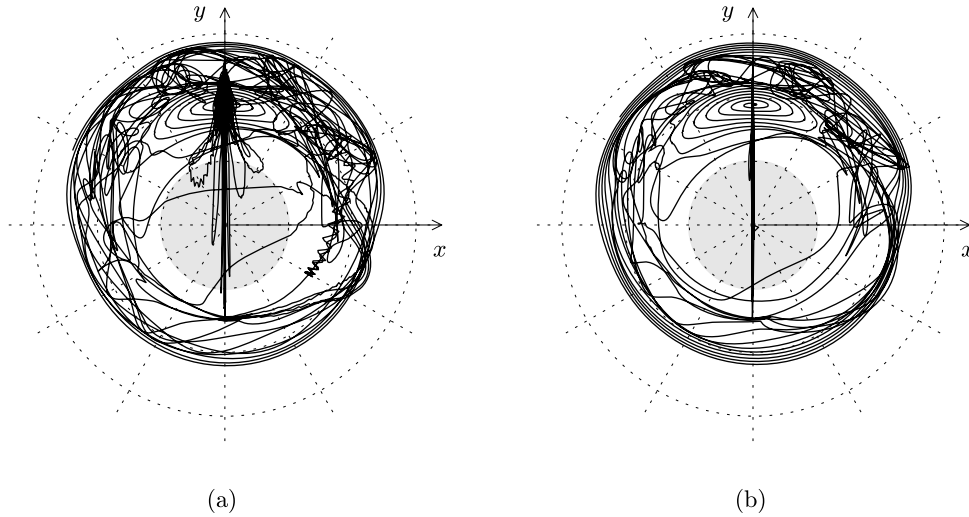


Figure 19: Orbit of a ball bearing (0 to 8 s); (a) Original bearing model, (b) Proposed bearing model.

for both bearings. The proposed bearing model is used in the calculations and the first 34 s of the response is presented. After the initial stage of the run-up (this time, the first 16 s) the radial displacement should gradually increase due to the higher angular velocity. However, another transient region appears around the 26th second of the simulation. A time span from 26 to 28 s represents the area (region C) where both bearings pass their clearance again. The system comes to its resonance, which causes a sudden movement of the shaft and consequently both bearings from one side to the other. Fig. 23 shows the orbits for the region C. A nonlinear dynamic bearing model is again the root cause of many numerical problems when performing a time integration. It is important to note that the system was not able to converge with the original bearing model. The presented scenario triggered our efforts to develop a modified dynamic bearing model that is able to surpass the shortcomings of the original model when performing a time integration.

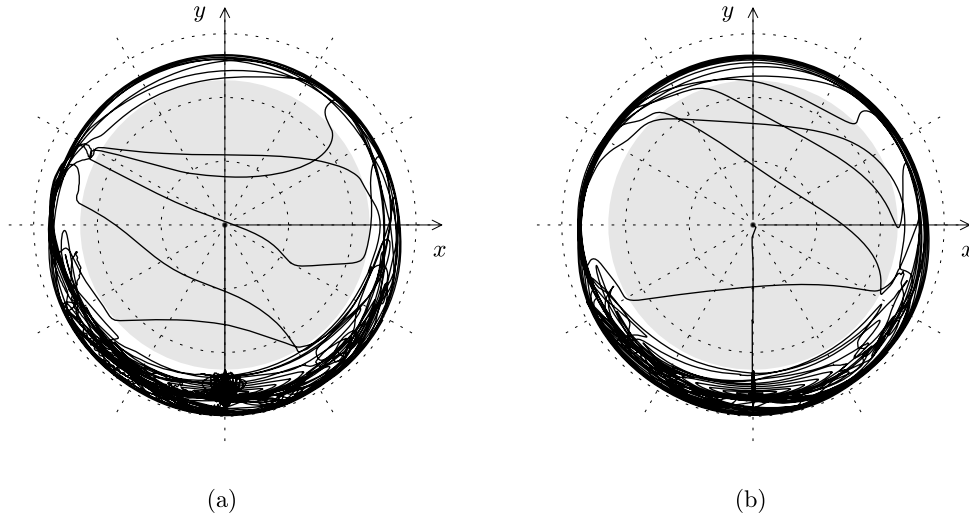


Figure 20: Orbit of a cylindrical roller bearing (0 to 8 s); (a) Original bearing model, (b) Proposed bearing model.

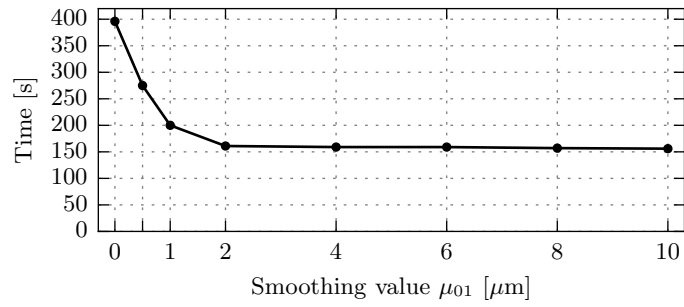


Figure 21: The effect of smoothing value μ_{01} on the overall computational time for the first 8 s of the simulation.

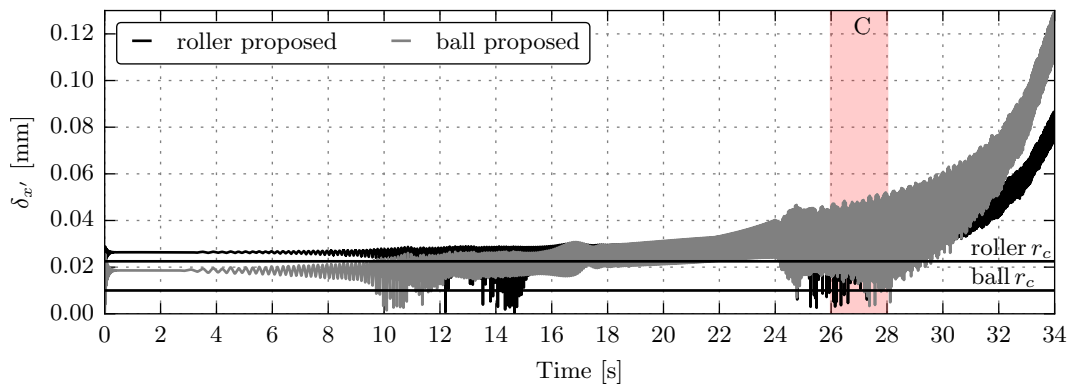


Figure 22: Radial response of both bearings with the proposed bearing model.

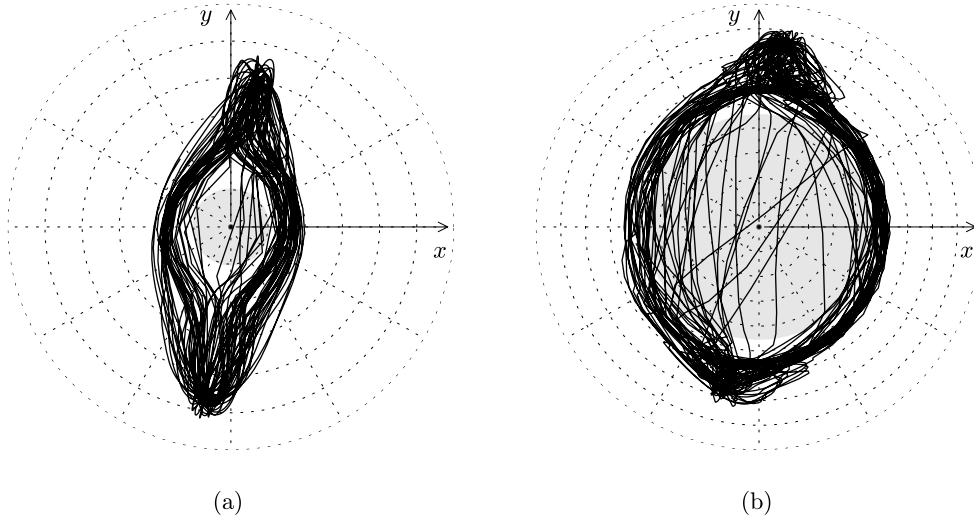


Figure 23: Orbits of the proposed bearing model (26 to 28 s); (a) Ball bearing, (b) Cylindrical roller bearing.

6. Conclusion

An improved dynamic model of rolling-element bearings is presented. The proposed bearing model is able to smooth the deformation-, force- and stiffness-displacement characteristics in the region of the contact-state transition. It is applicable for explicit calculations of the bearings that operate under radial clearance and are subjected to a dominant radial load. The smoothing is introduced in a modular manner, allowing a separate definition of a smoothing value to every single rolling element coming into a contact.

A simple case study of a shaft-bearing-housing assembly is presented and influence of a smoothing on the time integration procedure is studied. Two different regions of the system response are shown, i.e., the initial stage of run-up and the response near the resonance of the system. In both regions the bearings tend to pass their clearance. The response of a system containing the original bearing model is compared to the response of a system with the proposed bearing model. This could be done only for the initial stage of run-up, whereas the response close to the resonance of the system was not able to obtain with the original bearing model. It was shown that the proposed bearing model leads to a more stable calculation and a reduced computational time.

The presented work could be extended in a future to involve a time-varying bearing characteristics. Additionally, the smoothing of other than radial DOF could possibly be implemented. In fact, their contribution is in general much lower compared to the radial one; however, this would extend the applicability of the idea to all bearing types.

Acknowledgement

The authors would like to thank the ZF Friedrichshafen AG for supporting this research.

References

- [1] A. B. Jones, A general theory for elastically constrained ball and radial roller bearings under arbitrary load and speed conditions, *Journal of Basic Engineering*, ASME 82 (1960) 309–320.
- [2] T. A. Harris, *Rolling bearing analysis*, John Wiley, New York, 1984.
- [3] J. S. Rao, *Rotor dynamics*, John Wiley, New York, 1983.
- [4] M. F. While, Rolling element bearing vibration transfer characteristics: Effect of stiffness, *Journal of Applied Mechanics*, ASME 46 (1979) 677–684.
- [5] E. P. Gargiulo, A simple way to estimate bearing stiffness, *Machine design* 52 (1980) 107–110.

- [6] T. C. Lim, R. Singh, Vibration transmission through rolling element bearings, part 1: bearing stiffness formulation, *Journal of Sound and Vibration* 139 (2) (1990) 179–199.
- [7] T. C. Lim, R. Singh, Vibration transmission through rolling element bearings, part 5: Effect of distributed contact load on roller bearing stiffness matrix, *Journal of Sound and Vibration* 169 (4) (1994) 547 – 553.
- [8] T. J. Royston, I. Basdogan, Vibration transmission through self-aligning (spherical) rolling element bearings: Theory and experiment, *Journal of Sound and Vibration* 215 (5) (1998) 997–1014.
- [9] H. V. Liew, T. C. Lim, Analysis of time-varying rolling element bearing characteristics, *Journal of Sound and Vibration* 283 (2005) 1163–1179.
- [10] A. Gunduz, R. Singh, Stiffness matrix formulation for double row angular contact ball bearings: Analytical development and validation, *Journal of Sound and Vibration* 332 (22) (2013) 5898–5916.
- [11] D. S. Lee, D. H. Choi, A dynamic analysis of a flexible rotor in ball bearings with nonlinear stiffness characteristics, *International Journal of Rotating Machinery* 3 (1997) 73–80.
- [12] X. Sheng, B. Li, Z. Wu, H. Li, Calculation of ball bearing speed-varying stiffness, *Mechanisms and Machine Theory* 81 (2014) 166–180.
- [13] Y. Guo, R. G. Parker, Stiffness matrix calculation of rolling element bearings using a finite element/contact mechanics model, *Mechanism and Machine Theory* 51 (2012) 32–45.
- [14] S. M. Vijayakar, A combined surface integral and finite element solution for a three-dimensional contact problem, *International Journal for Numerical Methods in Engineering* 31 (1991) 524–546.
- [15] J. Zhang, B. Fang, J. Hong, S. Wan, Y. Zhu, A general model for preload calculation and stiffness analysis for combined angular contact ball bearings, *Journal of Sound and Vibration* 411 (Supplement C) (2017) 435 – 449.
- [16] T. C. Lim, R. Singh, Vibration transmission through rolling element bearings, part 2: system studies, *Journal of Sound and Vibration* 139 (2) (1990) 201–225.
- [17] T. C. Lim, R. Singh, Vibration transmission through rolling element bearings, part 3: geared rotor system studies, *Journal of Sound and Vibration* 152 (1) (1991) 31–54.
- [18] T. C. Lim, R. Singh, Vibration transmission through rolling element bearings, part 4: statistical energy analysis, *Journal of Sound and Vibration* 153 (1) (1992) 37–50.
- [19] X. Bai, Y. Wu, K. Zhang, C. Chen, H. Yan, Radiation noise of the bearing applied to the ceramic motorized spindle based on the sub-source decomposition method, *Journal of Sound and Vibration* 410 (2017) 35 – 48.
- [20] P. Čermelj, M. Boltežar, An indirect approach to investigating the dynamics of a structure containing ball bearings, *Journal of Sound and Vibration* 276 (2004) 401–417.
- [21] M. Razpotnik, T. Bischof, M. Boltežar, The influence of bearing stiffness on the vibration properties of statically over-determined gearboxes, *Journal of Sound and Vibration* 351 (2015) 221–235.
- [22] L.-X. Xu, Y.-G. Li, An approach for calculating the dynamic load of deep groove ball bearing joints in planar multibody systems, *Nonlinear Dynamics* 70 (3) (2012) 2145–2161.
- [23] L.-X. Xu, A general method for impact dynamic analysis of a planar multi-body system with a rolling ball bearing joint, *Nonlinear Dynamics* 78 (2) (2014) 857–879.
- [24] C. A. Fonseca, I. F. Santos, H. I. Weber, Influence of unbalance levels on nonlinear dynamics of a rotor-backup rolling bearing system, *Journal of Sound and Vibration* 394 (Supplement C) (2017) 482 – 496.
- [25] H. Wang, Q. Han, R. Luo, T. Qing, Dynamic modeling of moment wheel assemblies with nonlinear rolling bearing supports, *Journal of Sound and Vibration* 406 (Supplement C) (2017) 124 – 145.
- [26] A. Gunduz, J. T. Dreyer, R. Singh, Effect of bearing preloads on the modal characteristics of a shat-bearing assembly: Experiments on double row angular contact ball bearings, *Mechanical Systems and Signal Processing* 31 (2012) 176–195.
- [27] C. Bai, H. Zhang, Q. Xu, Effects of axial preload of ball bearing on the nonlinear dynamic characteristics of a rotor-bearing system, *Nonlinear Dynamics* 53 (3) (2008) 173–190.
- [28] D. P. Fleming, J. V. Poplawski, Unbalance response prediction for rotors on ball bearings using speed-and load-dependent nonlinear bearing stiffness, *International Journal of Rotating Machinery* 2005 (1) (2005) 53–59.
- [29] Z. Xia, G. Qiao, T. Zheng, W. Zhang, Nonlinear modeling and dynamic analysis of the rotor-bearing system, *Nonlinear Dynamics* 57 (4) (2009) 559–577.
- [30] R. I. Leine, N. v. d. Wouw, Stability and convergence of mechanical systems with unilateral constraints, *Lecture Notes in Applied and Computational Mechanics*, Springer, Dordrecht, 2008.